nature

SUPPLEMENTARY INFORMATION

https://doi.org/10.1038/s41586-019-1242-z

In the format provided by the authors and unedited.

# A cool accretion disk around the Galactic Centre black hole

Elena M. Murchikova[1,2]*, E. Sterl Phinney[2], Anna Pancoast[3] & Roger D. Blandford[4]

[1]Institute for Advanced Study, Princeton, NJ, USA. [2]Theoretical Astrophysics, Caltech, Pasadena, CA, USA. [3]Harvard-Smithsonian Center for Astrophysics, Cambridge, MA, USA. [4]Kavli Institute for Particle Astrophysics and Cosmology, Stanford University, Stanford, CA, USA. *e-mail: lena@ias.edu

## Supplementary Information

### Observations

The ALMA Cycle 3 observations of H30$\alpha$ line emission were obtained in April and August, 2016 for project 2015.1.00311.S. Observations were centered on Sgr A*: RA 17:45:40.0359, DEC -29:00:28.169 (J2000). They were conducted in receiver Band 6; the correlator was configured in the time division mode (TDM) with 4 spectrometers. Each spectrometer had a full bandwidth of 1875 MHz with 31.25 MHz resolution spectral channels. Because the width of the line was comparable to the bandwidth of the individual spectrometers, we overlapped two spectral windows centred at 231.058 GHz and 232.608 GHz (Supplementary Fig. 1). The remaining two spectral windows centred at 217.801 and 215.801 GHz were used to image the SgrA* continuum.

The observations were done primarily in ALMA configuration C40-5 with baselines up to 1.1 km and one execution was done in configuration C36-2/3 with baselines up to 460 m. For the C40-5 telescope configuration, good flux recovery is expected out to scales of $\sim 3.4$ arcsec and for C36-2/3 it is expected up to $\sim 10.7$ arcsec. Extended emission with spatial size greater than this will be partially resolved out. The data were taken with 43 12m antennas, using the total of 5.1 hours ALMA time, including calibrations. The integration time on target was 1.6 hours. The synthesized beam size was $0.29 \times 0.22\,\mathrm{arcsec}^2$ with PA= 6 degrees. J1924-2914 was used as a bandpass calibrator. J1744-3116 or J1717-3342 were used as phase calibrators. J1924-2914 or J1733-1304 were used as flux calibrators. The $1\sigma$ (rms) sensitivity was 0.3 mJy beam$^{-1}$ in each 40 km s$^{-1}$ channel. The observed line width was $\Delta V = 2,200\,\mathrm{km\,s^{-1}}$, with a velocity resolution of $40\,\mathrm{km\,s^{-1}}$.

Following delivery of data products, the data were re-reduced and imaged using the Common Astronomy Software Applications package (CASA). We did not perform self-calibration to preserve astrometry. The analysis was performed in Python and Mathematica.

The velocities given here are $V_{\mathrm{radio}} = c\frac{\nu_{\mathrm{rest}}-\nu}{\nu_{\mathrm{rest}}}$ relative to the LSRK. The Sgr A* observations were centred on $V_{\mathrm{LSR}} = 0.0\,\mathrm{km\,s^{-1}}$.

### Continuum Subtraction

The continuum subtraction is the crucial part of the analysis. Here we go through it in detail.

We observed a $2,200\,\mathrm{km\,s^{-1}}$ wide line emission with mean flux 1.7 mJy on top of the $\sim 2.8-3.5$ Jy, primarily from variable Sgr A* synchrotron continuum. To achieve this we needed excellent bandpass calibrations, which were repeated at least every 30 minutes.

Spectral setup: The width of the observed recombination line is comparable with the width of the single spectral window. Therefore, the line had to be observed in two spectral windows to achieve secure coverage of the full line width and quality continuum subtraction.

Spectral windows misalignment: The ALMA spectral windows are calibrated separately, and there is usually a small misalignment between the absolute value and the spectral slope of the data taken with one spectrometer (i.e. in one spectral window) with respect to the other. To ensure that separate spectral windows were consistently aligned, we positioned spectrometers with overlap. The overlap was established using 35 side channels in each spectral window.

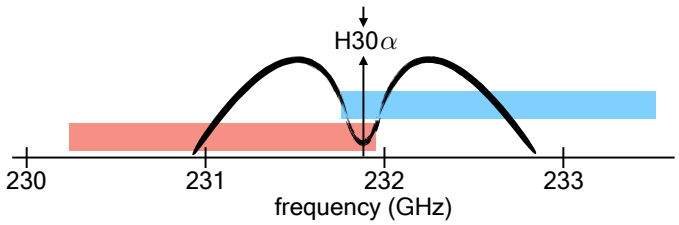


Supplementary Figure 1: **Spectral windows configuration for our ALMA Cycle 3 observations.** The observations have two spectral windows (blue and red) positioned across the line with an overlap. The frequency of the H30$\alpha$ line is marked with an arrow. The double peaked line between 231 GHz and 233 GHz is a schematic drawing of the detected line.

Because $\sim 10$ channels at the end of each spectral window are unusable this left us with $\sim 15$ useful channels to establish the proper alignment. The misalignment of the spectral windows in the delivered ALMA data and the necessity to establish the proper spectral window alignment during the data analysis require working with each spectral window separately.

Continuum subtraction procedure:

- Firstly, we imaged the data without continuum subtraction. The images were produced with the parameter Robust = 0.5. We cleaned images and identified the channels free of visible line features.
- Secondly, we performed u-v continuum subtraction using the identified channels, imaged the data again, and marked the channels with weak line features, which were not identified in the first step, to obtain a more accurate set of line free channels.
- Thirdly, we repeated the second step as many time as was necessary to identify all visible line features and achieve good continuum subtraction.
- When steps one through three are performed correctly in each spectral window the resulting continuum subtracted spectra will be aligned, i.e. the overlapping channels in each spectral window will match. In this work we achieved the alignment of the spectral windows with the u-v continuum subtraction procedure outlined above.

It is extremely important to establish the alignment of the separate spectral windows. Misaligned spectral windows will render further analysis nonsensical. However, the procedure described above is very time-consuming. The observed recombination line is wide which leaves a small number of channels grouped in a narrow spectral range at one of the ends of the spectral window for continuum subtraction. The channels have noise and the average obtained from them is not always accurate when interpolated across the whole spectral range. Adding or subtracting one channel to the list of "line-free channels" may affect the slope or the quality of the continuum subtracted spectrum.

A quicker procedure may be used to align the spectra instead. One may identify a reasonable list of the line-free channels (we quantitively define this below), do u-v continuum subtraction, clean the image with the CASA task TCLEAN, extract spectra in a selected aperture in each

spectral windows separately, and align the parts of the spectra by subtracting a straight line $a\nu + b$, with $a$ and $b$ constants, to match the overlapping parts of the spectra. (Due to the spectral window misalignment, the correct subtraction required different values $a$ and $b$ in each spectral window.)

We experimented with this procedure. We defined a reasonable list of the line-free channels to be one resulting in slopes of no more than $< 30$ mJy over the width of the spectral window after the u-v continuum subtraction. (Large slopes result in larger scatter of the points in the spectra. The trend observed in this experiment is that the task TCLEAN builds up the points at the top of the slope making them even higher.) After aligning the overlapping parts of the spectra we compared the join spectra obtained after u-v continuum subtraction with different sets of "line-free channels". The variations in the value of each point in the resulting line spectra were $\leq 7\%$. Therefore to those willing to undertake re-analysis of our data we recommend this procedure instead of the more tedious approach we took ourselves.

Regarding the identification of line-free channels, it is important to stress that the Galactic Center is a complex region containing stars, clouds and streamers moving with various velocities and therefore molecular line features are shifting in the velocity space from one spatial location to the other. This render identification of a unique set of line-free channels applicable everywhere across the region impossible. This, in general, is not an issue for strong line features. However, in the case of weak emission, such as the one we discuss in this work, it poses a problem. The shifting molecular features have flux comparable to or stronger than the line itself, and when (partially) shifted into the identified set of the line-free channels would drastically influence the quality of the continuum subtraction. In this work, we identified the reasonable list of the line-free channels only within $< 1$ arcsec around Sgr A*. We tested it within the aperture comparable to the beam size.

**Reliability**

To further test the reliability of our results we performed the following:

- We split the data into separate observation blocks (separate ALMA executions made on different days) and processed them independently without reference to each other. In each execution the value of the continuum was different and varied from $\sim 2.8$ Jy to $\sim 3.5$ Jy. In all cases we recovered the similar line shape, spectral width, the peak recombination line flux, and integrated line flux, excluding the possibility of the calibration artifact, as the calibration artifact would have a multiplicative effect on the observed spectra;

- We observed a continuum source J2000-1748, which was calibrated in the same way as Sgr A*, to check for possible technical or data reduction errors. No spectral feature analogues to those in Fig. 1 were detected, i.e. no double peaked line with wings of the width $\sim 1000\,\mathrm{km\,s^{-1}}$;

- We analysed ALMA Cycle 4 observations of Sgr A* conducted a year later on the same line, but with different spectral windows setup. All four spectra windows were positioned in one side band and with the overlap of $\sim 1/3$ of the spectra window width. There are three spectral windows across the observed recombination line). We recovered the similar

line shape, spectral width, the peak recombination line flux, and integrated line flux. The integrated line flux was larger by 10% compare to the Cycle 3 data presented here. Joint analysis of ALMA Cycle 4 and Cycle 5 observations will be published separately;

- Our ALMA Cycle 4 observations also had a continuum source – J1752-2956 (different from the one in the Cycle 3 observations), which was calibrated in the same way as Sgr A*, to check for possible technical or data reduction errors. No spectral feature analogues to those observed on Sgr A* spectra were detected.

**Estimation of Uncertainties**

- The extent of the emission is determined by analyzing the spectra within different apertures. An increase in the aperture size beyond $0.63 \times 0.51\,\mathrm{arcsec}^2$ does not increase the H30$\alpha$ flux within it. Emission outside of this region, if any, is $< 10\%$ of that inside.

- The observational sensitivity is $\delta S = 0.3$ mJy in each 40 $\mathrm{km\,s^{-1}}$ channel. Given that the mean value of the detected line is 2.5mJy, this gives us 13% uncertainty.

- We estimate the average uncertainty due to variations in u-v continuum subtraction and subsequent TCLEAN application at 5% on average (see section Continuum Subtraction).

- The overlapping parts of the spectra used to ensure proper spectral windows alignment do not match perfectly. They allow for variation in the alignment, specifically in the slopes of the aligning parts of the spectra (see section Continuum Subtraction). We estimate that the alignment uncertainty may result in $\sim 10\%$ variation of the velocity integrated line flux.

- The molecules with lines within $\sim 1$ GHz around H30$\alpha$ are acetone, methanol, sulfur dioxide $^{33}SO_2$, and similar complex molecules [8]. They are not expected to be present in substantial quantities in $10^4$ K gas. However, it is hard to exclude the possibility of narrow absorption or emission features from the foreground. The spectrum shows a relatively narrow $150\,\mathrm{km\,s^{-1}}$ bump at 231.43 GHz, which might be due to foreground emission. This feature is responsible for $0.2\,\mathrm{Jy\,km\,s^{-1}}$ in the total velocity integrated line flux of $S\Delta V_{\mathrm{H30}\alpha} = 3.8\,\mathrm{Jy\,km\,s^{-1}}$.

- We explore a relatively narrow spectral range of frequencies, while the wings of the line might extend further than $\pm 1000\,\mathrm{km\,s^{-1}}$ from the central frequency. In these observations we are unable to explore smooth and extended line features comparable in the velocity width to the width of the spectral window $\sim 2000\,\mathrm{km\,s^{-1}}$. This will be tested in our ALMA Cycle 5 observations which will be conducted in the spectral scan mode and cover $20,000\,\mathrm{km\,s^{-1}}$.

- We have expected higher noise than the one we are seeing in the spectra Fig. 1.

- The sharp dip at 230.9 GHz is robustly detected. So is the blue shifted wing of the line, which clearly rises from the flat continuum identified as the range between $-2000\,\mathrm{km\,s^{-1}}$ and $-1200\,\mathrm{km\,s^{-1}}$. The position of the redshifted wing is less certain due to the narrow

frequency range available between the CO line and the end of the band. The redshifted wing is positioned in place with the help of the overlapping spectral points which are mostly located in the dip.

- In the image made from the blue-shifted side of the spectrum, a negative intensity feature is present at the location of the reshifted emission. We will investigate this in our further data analysis with new data.

- It is hard to exclude the possibility that the dip in the middle is the result of the foreground absorption. There is a possible extended absorption feature at $\sim 230.9$ GHz to the West from Sgr A*. We will investigate this in our further data analysis with new data. A possibility also remains that the double-peaked line profile we see is noise or a combination of molecular lines. However, the combination of the following facts: that a similar spectral structure is detected both in ALMA Cycle 3 and in Cycle 4 (to be published separately), that regular structure is seen in the integrated blueshifted and redshifted emission, and that the width of the line emission is consistent with Keplerian velocity at the detected radius, makes us conclude that the chances of such a spectral structure appearing coincidentally at this frequency is quite low.

Combining the above factors we estimate that the combination of the listed above factors gives a combined uncertainty of $\sim 20\%$ of the value of each point on the presented continuum-subtracted line emission spectra, and an additional 10% uncertainty to the velocity integrated line flux due to the alignment of the separate spectral windows during which the curved representing the wings of the spectrum shift as the whole.

**Accretion onto Sgr A*, an overview.**

A supermassive black hole, Sagittarius A*, lies at the center of our Galaxy. It has mass $M_{\rm SgrA*} \simeq 4 \times 10^6 M_\odot$ [1, 2]. Building up such a massive black hole within the $\sim 10^{10}$ year lifetime of the Galaxy would require a mean accretion rate of $\sim 4 \times 10^{-4}\, M_\odot\, {\rm yr}^{-1}$. However, polarization measurements constrain the rate of gas accretion near the event horizon $R_s$ to $\dot{M}_{\rm horizon} \sim 10^{-9} - 10^{-7} M_\odot\, {\rm yr}^{-1}$ [26], and X-ray observations constrain it at the Bondi radius ($10^5\, R_{\rm s} = 0.04\, {\rm pc}$) to $\dot{M}_{\rm Bondi} \sim 3 \times 10^{-6} M_\odot\, {\rm yr}^{-1}$ [4, 5, 6]. If the radiative efficiency were $\sim 10\%$, the $\dot{M}_{\rm Bondi}$ would yield a luminosity $\sim 10^4$ times Sgr A*'s bolometric luminosity of a few $10^{36}\, {\rm erg\, s}^{-1}$ [31].

Extensive theoretical efforts have been put into resolving the mystery of Sgr A* accretion, and Radiatively Inefficient Accretion Flows (RIAF) in general. The models describe an accretion disk which cannot efficiently cool [10, 11] and is geometrically thick. The macroscopic effects transfer energy primarily to the ions. The ions lose only a small fraction of their energy to the electrons through Coulomb scattering on an inflow/heating timescale. As a result, the radiation efficiency of such a flow is very low, and the gas falling into the horizon radiates only $\ll 0.1 \dot{M} c^2$ (a radiatively efficient thin accretion disk radiates 6% - 42% of $\dot{M}c^2$ depending on the BH spin) [32, 33], allowing the observed luminosity to be produced by a much higher accretion rate than in a thin disk, while also explaining the mm to $\gamma-$ray spectrum [34].

An Advection-Dominated Accretion Flow (ADAF) [12] resembles a thick disk and rotates at an angular velocity much less than the Keplerian velocity $\Omega \ll \Omega_{\rm K}$. The small amount of radiation loss (the amount of energy transferred from ions to electrons) is estimated from Coulomb collisions, or set to be a free parameter to account for plasma effects. The black hole is fed at a constant rate and no material escapes. The density of such a disk scales as $\rho \sim r^{-\frac{3}{2}}$. However, an ADAF may be unstable to driving a wind. An Advection Dominated Inflow Outflow Solution (ADIOS) [13] is characterized by the presence of both an inflow and an outflow. It has the geometrical characteristics of the ADAF solution, but the disk has an accretion rate decreasing with radius as a power law, as the winds blow away material in the outer parts of the disk. The density profile $\rho \sim r^{-\frac{3}{2}+p}$, where $p$ is a constant parameter, is less steep than the ADAF, and the absolute value of the density is lower. ADAFs may be unstable to convection, so a Convection-Dominated Accretion Flow (CDAF) was proposed [14]. This accretion flow is marginally stable when the convection dominates advection in carrying the material inwards. A CDAF is also a thick disk rotating at a much lower angular velocity than Keplerian velocity, and feeds the black hole at a constant rate, but the density of such a flow scales as $\rho \sim r^{-\frac{1}{2}}$. We should also mention that in numerical simulations which included magnetic fields and a jet, it was obtained that $\rho \sim r^{-1}$ [16].

A detailed fit of no-wind ADAF models to the observed Sgr A* spectra from radio to $\gamma$-rays [35, 17] led to the estimate of the black hole accretion rate at

$$\dot{M}_{\rm SgrA*} = 7 \times 10^{-6} \left(\frac{\alpha}{0.3}\right) \frac{M_\odot}{\rm yr}, \tag{4}$$

where $\alpha$ is the dimensionless Shakura-Sunyaev viscosity parameter [36]. The no-wind ADAF causes a pile up of material in the accretion zone such that it becomes inconsistent with Faraday rotation measurements [26, 37, 38, 39]. Assuming that the magnetic field is ordered and at equipartition strength, the rotation measure constrains the accretion rate to a much lower value of

$$\dot{M} < 2 \times 10^{-7} \frac{M_\odot}{\rm yr}, \tag{5}$$

though the assumptions make this constraint rather model dependent.

Inclusion of an outflow solves the pile-up issue. The detailed fit of RIAF models with an outflow to the spectrum of Sgr A* from radio to $\gamma$-rays [18] results in

$$\dot{M}_{\rm Bondi} \sim 3 \times 10^{-6} M_\odot/{\rm yr} \tag{6}$$

$$\dot{M}_{\rm SgrA*} = 1.2 \times 10^{-7} M_\odot/{\rm yr}, \tag{7}$$

which is consistent with the constraint from the Faraday rotation measurements. There is no observational evidence for the presence of an outflow near Sgr A*. There is, however, no evidence excluding such a possibility either. A recent hydrodynamic simulations of the inner accretion flow of Sgr A* fueled by stellar winds obtained [15]

$$\dot{M}_{\rm SgrA*} = 2.4 \times 10^{-8} \frac{M_\odot}{\rm yr} \left(\frac{R}{R_{\rm s}}\right)^{1/2}. \tag{8}$$

It has been difficult to favour or rule out any of these accretion models for Sgr A*, primarily due to the lack of model-independent observational constraints on the accreting gas behaviour between 10 and $10^5\,R_{\rm s}$. We would like to stress that we are talking about the constraints which do not rely on assuming particular scaling of the accretion flow properties with radius to make a prediction. Constraints on the accretion rate from the Faraday rotation measurements [26, 37, 38, 39] are model-dependent as they assume scaling of density and the magnetic field strength with radius as input parameters. Constraints on the average density of the accretion flow from the drag on the G2-object's orbit [29] employs the density scaling with radius of the accretion flow as $\sim r^{-1}$ and assumes the flow is not rotating, and thus it is also model-dependent.

In this work we constrain the quantity and the dynamic properties of the cool $T \ll 10^7\,{\rm K}$ gas in the accretion zone of Sgr A*. We would like to emphasise that although our estimations discussed in details below depend on the model of the cool disk, they do not assume a model for the accretion flow or the scaling of its parameters with radius.

**Velocity Integrated Line Flux and Volume Emission Measure.**

In this section, we treat recombination line emission in the conventional case of no background pumping, so no maser emission. The main text discusses the evidence from Br $\gamma$ limits for masing in the H30$\alpha$ line, and the resulting correction factor $\mathscr{M}$ to $\epsilon$H30$\alpha$ and the density inferred from the emission measure.

Supplementary Fig. 2 shows a schematic of the recombination line technique. The H30$\alpha$ line luminosity is given by an integration over the line emitting region

$$L_{\rm H30\alpha} = \int \epsilon_{\rm H30\alpha} n_e n_p d^3 r, \tag{9}$$

where $\epsilon_{\rm H30\alpha}$ is the emissivity of H30$\alpha$, which is a function of density and temperature, $n_e$ is the electron number density, $n_p$ is the proton number density, and $d^3r$ is the three dimensional integral over the emitting volume. The flux received by the telescope is

$$S_{\rm H30\alpha} = \frac{L_{\rm H30\alpha}}{4\pi D^2} = \frac{\int \epsilon_{\rm H30\alpha} n_e n_p d^3 r}{4\pi D^2}. \tag{10}$$

Here $D$ is the distance to the emitting source.

In realistic cases, this flux is spread over a range of frequencies due to motion within the gas. The integrated line flux is then

$$\int_{\nu_{\rm min}}^{\nu_{\rm max}} S_\nu d\nu = \left( \int_{V_{\rm min}}^{V_{\rm max}} S_\nu dV \right) \frac{\nu_{\rm obs}}{c} = (S\Delta V_{\rm H30\alpha}) \frac{\nu_{\rm obs}}{c} = \frac{\int \epsilon_{\rm H30\alpha} n_e n_p d^3 r.}{4\pi D^2}, \tag{11}$$

where $S_\nu$ is the line flux per unit frequency, $S\Delta V_{\rm H30\alpha}$ is the velocity integrated line flux, $c$ is the speed of light, and $V$ is the line of sight velocity corresponding to the observed frequency's Doppler shift from the rest frequency of the H30$\alpha$ line. We find

$$S\Delta V_{\rm H30\alpha} = \frac{\int \epsilon_{\rm H30\alpha} n_e n_p d^3 r}{4\pi D^2} \frac{c}{\nu_{\rm obs}}. \tag{12}$$

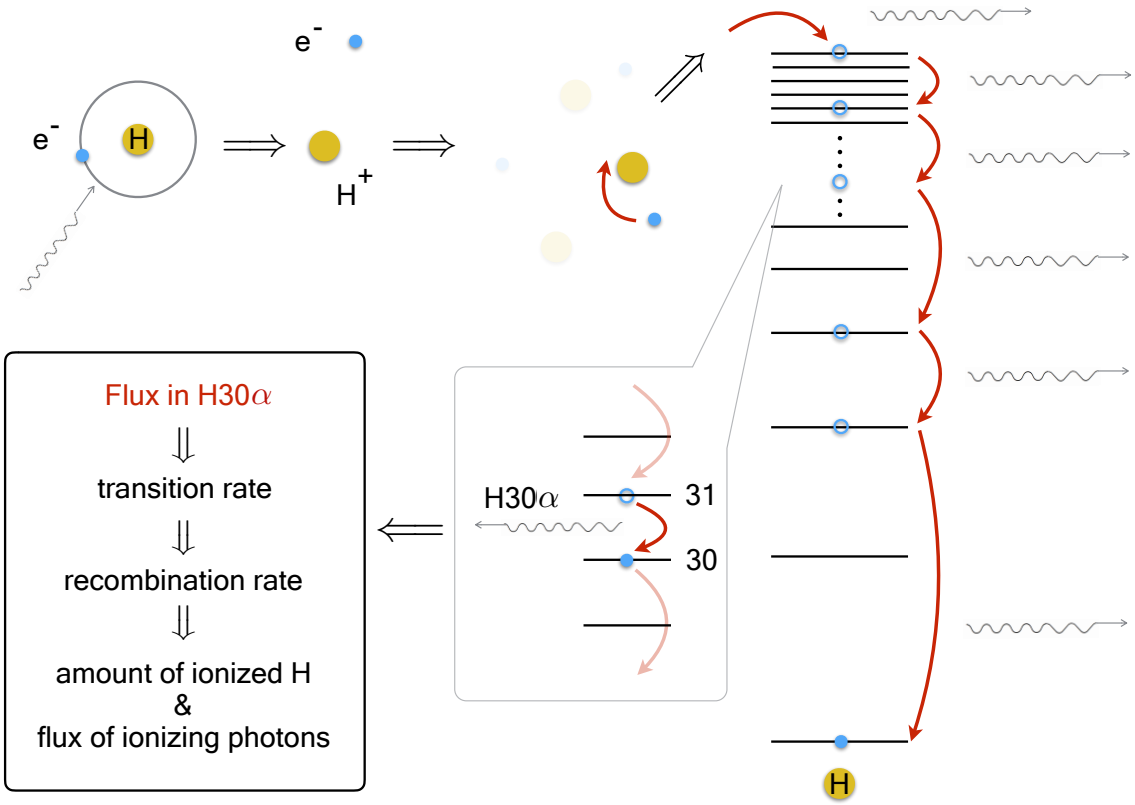


Supplementary Figure 2: **Schematic plot illustrating the recombination line technique.** If photons with energy $E_\gamma \geq 13.6$ eV are present, they ionize neutral hydrogen. As the electrons and protons recombine, some recombinations occur to $n \gg 1$. The electrons cascade down to the ground level. Some electrons pass through the levels of interest, in this case H30$\alpha$ : $n = 31 \rightarrow 30$, during the cascade. The amount of radiation coming out in H30$\alpha$ indicate how many H30$\alpha$ transitions are occuring, how many atoms are recombining, how much ionized material is in the region, and the background flux of the ionizing photons.

In a simplified case of an emitting region of constant density and temperature, this equation is reduced to

$$S\Delta V_{\rm H30\alpha} = \frac{\epsilon_{\rm H30\alpha} n_e n_p {\rm vol}}{4\pi D^2} \frac{c}{\nu_{\rm obs}}, \tag{13}$$

where $\mathrm{vol} = \int d^3r$ is the total volume in space occupied by the $10^4$ K gas. The emissivity $\epsilon_{\rm H30\alpha}(T, n)$ varies weakly with density $n$ [24]:

$$\epsilon_{\rm H30\alpha}(10^4\,{\rm K}, 10^4\,{\rm cm^{-3}}) = 1.05 \times 10^{-31}\,{\rm erg\,s^{-1}cm^3}, \tag{14}$$
$$\epsilon_{\rm H30\alpha}(10^4\,{\rm K}, 10^5\,{\rm cm^{-3}}) = 1.08 \times 10^{-31}\,{\rm erg\,s^{-1}cm^3}, \tag{15}$$
$$\epsilon_{\rm H30\alpha}(10^4\,{\rm K}, 10^6\,{\rm cm^{-3}}) = 1.25 \times 10^{-31}\,{\rm erg\,s^{-1}cm^3}, \tag{16}$$
$$\epsilon_{\rm H30\alpha}(10^4\,{\rm K}, 10^7\,{\rm cm^{-3}}) = 1.36 \times 10^{-31}\,{\rm erg\,s^{-1}cm^3}. \tag{17}$$

In what follows we assume

$$\epsilon_{\rm H30\alpha} \simeq \epsilon_{\rm H30\alpha}(10^4\,{\rm K}, 10^6\,{\rm cm^{-3}}). \tag{18}$$

Substituting equation 18, $\nu_{\rm obs} = \nu_{\rm H30\alpha} = 231.9$ GHz, $D_{\rm H30\alpha} = 8.0$ kpc, and $1\,{\rm Jy} = 10^{-23}\frac{\rm erg}{\rm s\,cm^2\,Hz}$ into equation 13 we find

$$S\Delta V_{\rm H30\alpha} = 2.1 \times 10^{-60} n_e n_p {\rm vol}\ {\rm Jy\,km\,s^{-1}} \tag{19}$$

and the expression for the volume emission measure is

$$\mathrm{EM} = n_e n_p {\rm vol} = S\Delta V_{\rm H30\alpha} \times 4.7 \times 10^{59}\ {\rm cm^{-3}}. \tag{20}$$

**Disk of a uniform density**

Let us consider a Shakura-Sunyaev disk model. For simplicity we assume $n = n_e = n_p = \mathrm{const}$. The disk properties are as follows: an isothermal disk at $T = 10^4$ K with an outer radius $R_{\rm max} = 0.23$ arcsec and an inner radius $R_{\rm min} = 0.07$ arcsec, a half opening angle $\phi$, such that $H/R = \tan\phi$, where $H$ is the scale height of the disk measured from the midplane to the top. The disk rotates with an azimuthal velocity $V_\Omega$ equal to the Keplerian velocity $V_{\rm K}$ ($V_\Omega = V_{\rm K}$).

The emission measure is given by

$$\mathrm{EM} = n^2 \frac{4}{3}\pi R_{\rm max}^3 \tan\phi \left[1 - \left(\frac{R_{\rm max}}{R_{\rm min}}\right)^3\right]. \tag{21}$$

Making use of equation 2 of the main text and its preceeding paragraph's definition of the factor $\mathscr{M}$ to account for possible masing, we find

$$n = \frac{1.5 \times 10^4}{\sqrt{\tan\phi}} \left(\frac{R_{\rm max}}{9\,{\rm mpc}}\right)^{-3/2} \left(\frac{\mathscr{M}}{100}\right)^{-1/2}\ {\rm cm^{-3}}, \tag{22}$$

$$M = 1.0 \times 10^{-3} \sqrt{\tan\phi} \left(\frac{R_{\rm max}}{9\,{\rm mpc}}\right)^{3/2} \left(\frac{\mathscr{M}}{100}\right)^{-1/2}\ M_\odot. \tag{23}$$

Then the mass accretion rate onto the black hole $\dot{M}$ is

$$\dot{M} = 2\pi R 2H(R) V_R \rho(R), \tag{24}$$

where $V_R$ is the radial inflow velocity of the gas at the radius R and $\rho = nm_p$ is the gas mass density. The expression for the radial inflow velocity in the accretion disk is

$$V_R = \alpha \left(\frac{H}{R}\right)^2 V_\Omega = \alpha \left(\frac{H}{R}\right)^2 \chi V_K, \tag{25}$$

where $c_s$ is the speed of sound and $\alpha$ is the dimensionless Shakura-Sunyaev viscosity parameter [36] and $\chi = V_\Omega / V_K$ is the parameter describing deviation of disk's material orbital velocity from Keplerian velocity. We find that the accretion rate at the radius $R_{\rm mean} = (R_{\rm max} + R_{\rm min})/2$ is

$$\begin{aligned} \dot{M} &= 4\pi R^2 n m_p \chi V_K \alpha \left(\frac{H}{R}\right)^3 \\ &= 3.2 \times 10^{-5} \left(\tan\phi\right)^{5/2} \chi \left(\frac{\alpha}{0.1}\right) \left(\frac{\mathscr{M}}{100}\right)^{-1/2} \frac{M_\odot}{\rm yr}. \end{aligned} \tag{26}$$

The scale height of the disk can be estimated using

$$\tan\phi = \frac{H}{R} = \frac{c_{\rm s}}{V_\Omega}. \tag{27}$$

The speed of sound in the ideal gas is

$$c_s = \sqrt{\frac{\gamma p}{\rho}} = \sqrt{\frac{\gamma (n_e + n_p) k_B T}{n_p m_p}} = \sqrt{\frac{\gamma 2 k_B T}{m_p}} = 16.6 \left(\frac{T}{10^4\,{\rm K}}\right)^{1/2} \ {\rm km\,s^{-1}}, \tag{28}$$

then

$$\tan\phi = \frac{c_{\rm s}}{V_\Omega} \simeq \frac{16.6\ {\rm km\,s^{-1}}}{2,000\ {\rm km\,s^{-1}}} \sim 0.01 \left(\frac{T}{10^4\,{\rm K}}\right)^{1/2}. \tag{29}$$

Finally we have

$$n = 1.5 \times 10^5 \left(\frac{T}{10^4\,{\rm K}}\right)^{-1/4} \left(\frac{R_{\rm max}}{9\,{\rm mpc}}\right)^{-3/2} \left(\frac{\mathscr{M}}{100}\right)^{-1/2} \ {\rm cm^{-3}} \tag{30}$$

$$M = 1.0 \times 10^{-4} \left(\frac{T}{10^4\,{\rm K}}\right)^{1/4} \left(\frac{R_{\rm max}}{9\,{\rm mpc}}\right)^{3/2} \left(\frac{\mathscr{M}}{100}\right)^{-1/2} \ M_\odot \tag{31}$$

$$\dot{M} = 2.7 \times 10^{-10} \left(\frac{\chi}{1}\right) \left(\frac{T}{10^4\,{\rm K}}\right)^{5/4} \left(\frac{\alpha}{0.1}\right) \left(\frac{\mathscr{M}}{100}\right)^{-1/2} \ \frac{M_\odot}{\rm yr}. \tag{32}$$

A disk with these properties is gravitationally stable, since the Toomre $Q$ in the centre of the structure is much greater than one: $Q = \frac{V_{\rm K}/R c_s}{\pi G m_p n H} \sim 1.7 \times 10^7 \gg 1$ .

**BLR-like Ensemble of Clouds.**

It is easier for a maser explanation of the difference in emissivity inferred from these observations and the preliminary Br$\gamma$ estimates if the beam filling factor is low. This suggests consideration of a disk of cloudlets.

Let us consider a thick disk consisting of Broad-Line-Region (BLR)-like cloudlets. The model is as follows: a disk with an outer radius $R_{\rm max} = 0.23$ arcsec and an inner radius $R_{\rm min} = 0.07$ arcsec, a half opening angle $\phi$, such that $H/R = \tan\phi$, where $H$ is the scale height of the disk measured from the midplane to the top, filled with isothermal cloudlets at $T \sim 10^4$ K. The cloudlets have a characteristic radius $r$, an internal density $n = n_e = n_p$ and they move in circular orbits with velocities proportional to Keplerian velocities $V_\Omega = \chi V_{\rm K}$ with $\chi \in (0, 1]$. The volume of such a disk is

$$\mathrm{vol}_{\rm disk} = \frac{4}{3}\pi \tan\phi R_{\rm max}^3 \left(1 - \frac{R_{\rm min}^3}{R_{\rm max}^3}\right), \tag{33}$$

and the volume emission measure is

$$\mathrm{EM} = n^2 \times \mathrm{vol}_{\rm cloud} \times n_{\rm cloud} \mathrm{vol}_{\rm disk}. \tag{34}$$

The accretion is due to cloudlet collisions, during which they lose angular momentum and an amount of material, approximately equal to the mass of a cloudlet, "rains" down on the black hole. The collision rate per cloud is

$$z_{\rm cloud} = \pi r^2 \times \chi \frac{H}{R} V_{\rm K} \times n_{\rm cloud}. \tag{35}$$

Here $n_{\rm cloud}$ is the number density of the cloudlets within the disk, and $\chi \frac{H}{R} V_{\rm K}$ is the velocity of the clouds relative to each other.

The mass accretion rate for such a disk is independent of its opening angle $\tan\phi$ :

$$\dot{M} = m_{\rm cloud} \times z_{\rm cloud} \times n_{\rm cloud} \mathrm{vol}_{\rm disk} \tag{36}$$

$$= \frac{\mathrm{EM}^2}{\mathrm{vol}_{\rm disk}/\tan\phi} \frac{m_p \chi V_{\rm K}}{4 r n^3} \tag{37}$$

$$= 1.2 \times 10^{-7} \left(\frac{\chi}{1/4}\right) \left(\frac{n}{10^6\,\mathrm{cm}^{-3}}\right)^{-3} \left(\frac{r}{9\mu\mathrm{pc}}\right)^{-1} \left(\frac{R_{\rm max}}{9\,\mathrm{mpc}}\right)^{-7/2} \left(\frac{\mathscr{M}}{100}\right)^{-2} \frac{M_\odot}{\mathrm{yr}}. \tag{38}$$

Here we used $r = 10^{-3} R_{\rm max} = 9\mu$pc as a characteristic size of cloudlets, $V_{\rm K}$ at the mean radius of the disk $R_{\rm mean} = (R_{\rm max} + R_{\rm min})/2 = 0.15$ arcsec, and $\chi = 1/4$ as it is the ratio between the velocity where the most emission comes from $V_\Omega \simeq 500\,\mathrm{km\,s^{-1}}$ and Keplerian velocity $V_{\rm K} \simeq 2,000\,\mathrm{km\,s^{-1}}$ at $R_{\rm mean}$. The mass of this disk is

$$M_{\rm disk} = m_p \frac{EM}{n} = 1.5 \times 10^{-5} \left(\frac{\mathscr{M}}{100}\right)^{-1} \left(\frac{n}{10^6\,\mathrm{cm}^{-3}}\right)^{-1} M_\odot. \tag{39}$$

The mass of the cloudlet is

$$m_{\rm cloud} = m_p n \frac{4}{3}\pi r^3 = 7 \times 10^{-11} \left(\frac{n}{10^6\,\mathrm{cm}^{-3}}\right) \left(\frac{r}{9\mu\mathrm{pc}}\right)^3 M_\odot. \tag{40}$$

The number density of cloudlets in the disk is

$$n_{\rm cloud} = \frac{M_{\rm disk}/m_{\rm cloud}}{{\rm vol}_{\rm disk}} \simeq \frac{70}{\tan\phi}\,{\rm mpc}^{-3}. \quad (41)$$

The lifetime of the disk strongly depends on the assumed density within the cloudlets. For $n = 10^6\,{\rm cm}^{-3}$, the disk has to be replenished with $10^4\,{\rm K}$ gas supplied by the circumnuclear torus and the mini-spiral and/or the cooling of colliding winds in order to exist beyond $\sim 120$ years. The gas supplied form by the cool gas structures around the Galactic Center [19] has to survive the hot environment near the black hole without being complete evaporated. While hot gas has to be able to cool on the reasonable timescale. The average density of the gas in the hot estimated accretion flow is estimated at $\sim 10^2 - 10^3\,{\rm cm}^{-3}$ at the radius of the disk [15]. However if colliding stellar winds create overdensities $\sim 10^6\,{\rm cm}^{-3}$, such clumps would cool from $10^7\,{\rm K}$ on faster than the dynamic timescale up to the $R < R_{\rm disk}$. Should the density within the clump be a little higher the lifetime could easily be 1000 year. For a long-lived disk there is of course a possibility that the disk was formed from a one-time infall event. However we think that replenishing is more likely a continuous process as the Galactic Center is a complex region with no shortage of gas supply either hot or cold.

**BLR-like Ensemble of Clouds. Modelling.**

If the gas disk is similar to the BLR in active galactic nuclei (AGN), we can model the geometry and dynamics of the gas emission using a method applied to the optical H$\beta$ broad emission line [27, 28]. The model assumes an ionizing photon source located at the location of SgrA*, an outer radius of emission less than 10 light days (corresponding to the spectrum aperture), and a black hole mass of $4.0 \times 10^6 M_\odot$. Fitting the H30$\alpha$ emission line to within the spectral uncertainties tightly constrains the BLR model parameters as shown in Supplementary Fig. 3. The dynamics are dominated by outflowing orbits with more tangential than radial velocities, a result that is consistently inferred even if the black hole mass is left as a free model parameter or the outer radius of emission is larger than 10 light days. The geometry parameters are much more sensitive to the value of black hole mass and the maximum radius of emission, due to degeneracies between the disk thickness, radial size, and orientation with the black hole mass. The inferred geometry is a slightly thick disk viewed close to face-on and with a ratio of the mean radius to the minimum radius of emission inferred to be 1.78. Although the input to the modelling code was only the H30$\alpha$ line spectrum, it infers disk properties similar to the ones we deduce from the imaging. These results also hint at an observational signature of outflow in the Galactic Centre.

The red/blue shifted emission we observe might be due a bipolar outflow, rather than a rotating disk. This scenario is disfavoured in our modelling, however it cannot be completely ruled out. Future higher resolution observations could help to distinguish these cases.

**Ionization Equilibrium**

For the material in the disk to be ionized, we need an ionizing photon flux large enough to counteract the recombination loses is needed. Assuming that the disk is in equilibrium, i.e.,

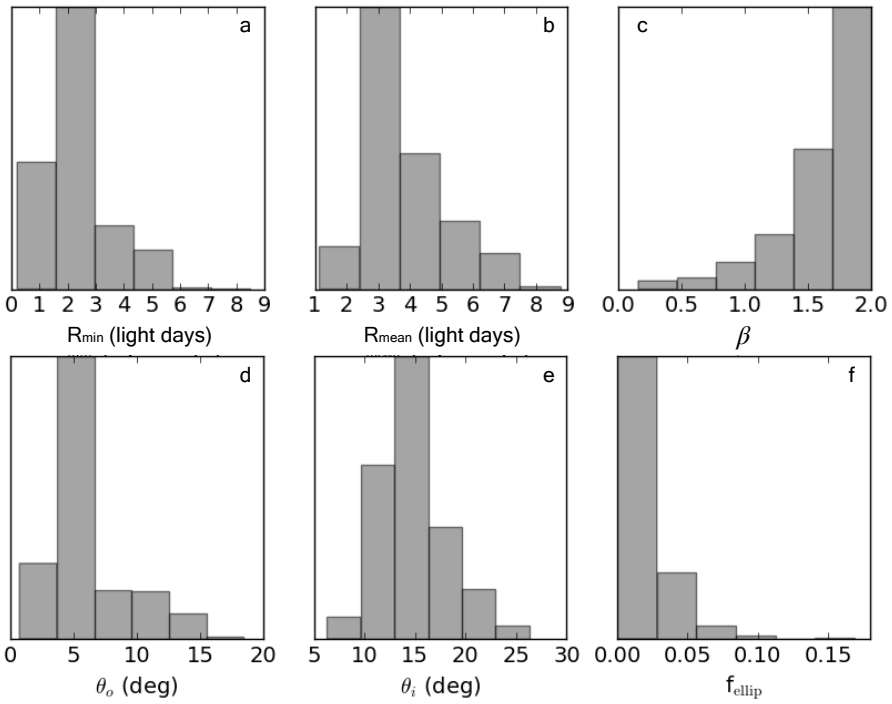


Supplementary Figure 3: **Inferred posterior probability distributions for key BLR model parameters.** The radial distribution of line emission is described by the three parameters in the top row, including (a) the minimum radius of emission $R_{\rm min}$, (b) the mean radius of emission $R_{\rm mean}$, and (c) the Gamma distribution shape parameter $\beta$, where the radial profile of emission is $\propto x^{1/\beta^2-1}\exp(-x)$. Values of $\beta \rightarrow 0$ correspond to a narrow Gaussian-like radial profile, while $\beta = 1$ corresponds to an exponential profile and $\beta > 1$ (as preferred by the data) corresponds to a profile that decreases more steeply than exponentially with radius. The median value and 68% confidence intervals for the ratio of the mean radius to the minimum radius are $1.78^{+0.22}_{-0.30}$. The opening angle $\theta_o$ (d) is slightly thick, where $\theta_o = 0$ (90) deg is a perfectly thin disk (sphere). The inclination angle $\theta_i$ (e), at which an observer views the disk, is inferred to be close to face-on, where $\theta_i = 0$ (90) deg is perfectly face-on (edge-on). The fraction of line emission from gas on near-circular orbits (f), $f_{\rm ellip}$, is generally less than 10%, with the remaining gas in outflowing orbits having predominantly tangential, instead of radial, velocities. In addition to the posterior PDFs shown here, the geometry of emission is inferred to have some asymmetries in the angular coordinate direction, including more emission from the far side of the disk further from the observer and also more emission from above the disk mid-plane. Combining these two forms of asymmetry, the brightest part of the disk is the far side above the disk mid-plane.

that the number of recombinations per unit time is equal to the number of ionizations, we find

$$Q_0 = \int \alpha_B n_p n_e d^3 r \simeq \alpha_B \mathrm{EM}. \tag{42}$$

Here $Q_0$ is the flux of ionizing photons with energies $E_\gamma > 13.6$ eV, and $\alpha_B$ is the sum of the recombination coefficients to all levels n $\geq 2$. (The so-called Case B recombination: recombinations to n $\geq 2$ result in the destruction of an ionizing photon.) Using $\alpha_B(T = 10^4\mathrm{K}) = 2.59 \times 10^{-13}\,\mathrm{cm}^3$, we find

$$Q_0 = 4.6 \times 10^{45} \left(\frac{\mathscr{M}}{100}\right)^{-1} \mathrm{s}^{-1} \tag{43}$$

or

$$L_{\mathrm{EUV}} = 1 \times 10^{35}\,\mathrm{erg\,s}^{-1} \sim \frac{L_{\mathrm{bol}}}{30}. \tag{44}$$

This is $\sim 1/30$ of the bolometric luminosity of Sgr A*, which is larger than expected from Sgr A* [34]. Thus we do not expect all of this ionizing flux to be coming from the black hole itself.

An additional source of ionizing photons is the surrounding stars. We assume that most of the ionizing flux from the stars (S. Ressler and E. Quataert (private communication)) [40, 15] comes from 15 Wolf-Rayet (WR) stars in orbits of $\sim 4$ arcsec. Most of these stars belong to the counterclockwise disk. The bolometric luminosity of WR stars ranges from $L_{\mathrm{WR}} \sim 10^5 - 10^6 L_\odot$ and we expect $\sim 39\% - 69\%$ of this luminosity to be emitted at $E_\gamma \geq 13.6$ eV [41]. Near the mean radius of the disk these 15 WR stars produce an ionizing photon flux of

$$Q_0^{\mathrm{WR}} \sim \left(\frac{2}{\pi}\right)^2 \times \frac{15 \times 10^5 L_\odot \times 0.55}{13.6 \times 1.6 \times 10^{-12}} \times \frac{\pi(0.23\,\mathrm{arcsec})^2 - \pi(0.07\,\mathrm{arcsec})^2}{4\pi(4\,\mathrm{arcsec})^2} \sim 2 \times 10^{46}\,\mathrm{s}^{-1}, \tag{45}$$

where $(2/\pi)^2$ is a geometrical factor accounting for the disk inclination with respect to the illuminating stars. Note that $Q_0^{\mathrm{WR}}$ is an upper limit, since the characteristics of WR stars are uncertain and the emitted EUV would sustain considerable losses before reaching the disk. Thus we conclude that the ionizing photon flux required to keep the disk ionized is a collective effect of Sgr A* and nearby orbiting stars.

**The disk and the G-objects.**

We now consider the possible effect of our disk of ionized hydrogen on the orbit of the G-objects near Sgr A*. The physical properties of G2, and G-objects in general, are uncertain. Some say they are gravitationally unbound gas and dust clouds of a few $M_{\mathrm{Earth}}$ and $\sim 100$ au radius [42, 29], while the others argue they are stars embedded in few au dusty envelopes which in turn are embedded in even larger Br$\gamma$ emitting envelopes and originate from stellar mergers [21, 20]. The latter approach avoids the necessity of postulating that G2 assembled itself in its compact form right at the moment when its detection became possible with introduction of new adaptive optics, it addresses the object's compactness and absence of tidal distortion during

the close passage by Sgr A* in $L'$ broadband filter (which traces the dust emission) [21, 20], and naturally explains that its brightness did not change over the decade.

Here we consider a toy model – a cloud of mass $\sim 3M_{\rm Earth}$ and radius $r_{\rm G2} = 0.015\,{\rm arcsec} = 60\,{\rm au}$ [22, 29]. In the case that G2 has a cloudy nature this would represent the whole object. In the case of a stellar G2, this would represent its extended Br$\gamma$ emitting envelope, which takes the hit during the interaction with the disk. The much heavier central star and its surrouding few au dust shell passes through the disk with no noticeable interaction. During the collision the disk is treated as stationary. The spherical clouds collide with it at the mean radius of the disk and at a right angle to its plane .

An encounter with the thin disk (Methods section "Disk of a uniform density") is roughly equivalent to an aluminium ball 1 cm in diameter passing through a 1 mm layer of water, as $r_{\rm G2}/H_{\rm disk} = 10$ and $n_{\rm G2}/n_{\rm disk} = 2.9$. When such a cloud passes through the mean radius of the disk it loses $\sim 1\%$ of its orbital momentum:

$$\Delta P_{\rm G2} = F_{\rm drag}\Delta t \sim -\frac{1}{4}\pi r_{\rm G2}^2 v_{\rm G2}^2 \frac{2H}{v_{\rm G2}} \sim -P_{\rm G2} \times \frac{3}{8}\frac{H}{r_{\rm G2}}\frac{\rho_{\rm disk}}{\rho_{\rm G2}} \sim -\frac{P_{\rm G2}}{100}, \quad (46)$$

$$\Delta L_{\rm G2} \sim 0.01 L_{\rm G2}. \quad (47)$$

Here we used $P_{\rm G2} = m_{\rm G2}v_{\rm G2}$, $L_{\rm G2} = R_{\rm mean} \times P_{\rm G2}$, $F_{\rm drag} = -\frac{1}{2}A_{\rm eff}C\rho_{\rm disk}v_{\rm G2}^2$, an effective area of the cloud is $A_{\rm eff} = \pi r_{\rm G2}^2$, the drag coefficient $C \sim 1/2$ for a ball-like cloud, the duration of the encounter is $\Delta t = 2H/v_{\rm G2}$, $H/R = 0.01$, and $R_{\rm mean} = 0.15\,{\rm arcsec}$.

An encounter with the clumpy BLR-like disk (Methods section "BLR-like Ensemble of Clouds") is roughly equivalent to 1 mm aluminium bullets piercing a 10 cm in diameter water ball, as $r_{\rm G2}/r_{\rm clouds} \sim 100$ and $n_{\rm cloudlets}/n_{\rm G2} = 2.3$. When G2 passes through the disk composed of bullet-cloudlets it loses $\sim 2\%$ of its orbital momentum:

The loss due to one encounter is

$$\Delta P_{\rm G2} = F_{\rm drag}\Delta t \sim -\frac{1}{4}\pi r_{\rm clouds}^2 v_{\rm G2}^2 \frac{r_{\rm G2}}{v_{\rm G2}} = -P_{\rm G2} \times \frac{3}{16}\left(\frac{r_{\rm clouds}}{r_{\rm G2}}\right)^2 \sim -P_{\rm G2} \times 2 \times 10^{-5}. \quad (48)$$

There are $\sim 10^3$ bullet-cloudlets piercing the ball:

$$N_{\rm collisions} = n_{\rm clouds} \times \pi r_{\rm G2}^2 \times 2H \sim \frac{70}{\tan\phi} \times \pi r_{\rm G2}^2 \times 2R_{\rm mean}\tan\phi \sim 10^3, \quad (49)$$

resulting in a total loss of angular momentum of $\Delta L_{\rm G2}^{\rm total} = R_{\rm mean}\Delta P_{\rm G2} N_{\rm collisions} \sim 0.02 L_{\rm G2}$. This can be less if the internal density of the cloudlets is higher.

The momentum loss of G2 and the disk damage due to the encounter can be zero, if G2 does not interact with the disk at all. This is possible. The closest approach of G2 to Sgr A* is $\sim 200\,{\rm au} = 0.025\,{\rm arcsec}$, while the disk has a hole in the middle of the radius size $\sim 0.1\,{\rm arcsec}$ through which G2 can safely pass and avoid the interaction completely. Such a scenario would constrain the disk plane. The loss of less than a few percent of the G2's orbital momentum due to the encounter with the disk is within the uncertainties of determining G2's orbital parameters [29].

When the properties of the disk are better determined and the motion of G2 is more accurately constrained, these two objects could constrain properties of each other. At the moment no meaningful constraint can be set on the disk from the motion of G2.

Note that the G1 object faded away $\sim 4-5$ years after its pericenter in 2001, and is believed to have been tidally stripped [20]. The loss of the envelope occured at a similar distance from Sgr A* in the plane of the sky as the disk reported here. Unfortunately, no observations prior to or at the time of the G1 close passage are available.

## References


[31] Narayan, R., et al. Advection-dominated accretion model of Sagittarius A*: evidence for a black hole at the Galactic center, Astrophys. J., 492, 554 (1998)

[32] Thorne, K. S. Disk-Accretion onto a Black Hole. II. Evolution of the Hole, Astrophys. J., 191, 507-520 (1974)

[33] Novikov, I. D. and Thorne, K. S. Astrophysics of black holes, Black Holes (Les Astres Occlus), 343-450 (1973)

[34] Narayan, R. and Yi, I. and Mahadevan, R. Explaining the spectrum of Sagittarius A* with a model of an accreting black hole, Nature, 374, 623-625 (1995)

[35] Mahadevan, R. and Narayan, R. and Krolik, J. Gamma-Ray Emission from Advection-dominated Accretion Flows around Black Holes: Application to the Galactic Center, Astrophys. J., 486, 268-275 (1997)

[36] Shakura, N. I., & Sunyaev, R. A. Black holes in binary systems. Observational appearance, Astron. Astrophys., 24, 337-355 (1973)

[37] Aitken, D. K. Detection of Polarized Millimeter and Submillimeter Emission from Sagittarius A*, Astrophys. J. Lett., 534, L173-L176 (2000)

[38] Agol, E. Sagittarius A* Polarization: No Advection-dominated Accretion Flow, Low Accretion Rate, and Nonthermal Synchrotron Emission, Astrophys. J. Lett., 538, L121-L124 (2000)

[39] Marrone, D. P. and Moran, J. M. and Zhao, J.-H. and Rao, R. An Unambiguous Detection of Faraday Rotation in Sagittarius A*, Astrophys. J. Lett., 654, L57-L60 (2007)

[40] Martins, F. et al. Stellar and wind properties of massive stars in the central parsec of the Galaxy, Astron. Astrophys., 468, 233-254 (2007)

[41] Crowther, P. A. Physical Properties of Wolf-Rayet Stars, Ann. Rev. Astron. Astrophys., 45, 177-219 (2007)

[42] Gillessen S., et al., A gas cloud on its way towards the supermassive black hole at the Galactic Centre, Nature, 481, 51 (2012)

[43] Pfuhl, O., et al. The Galactic Center Cloud G2 and its Gas Streamer Astrophys. J., 798, 111 (2015)

[44] Burkert A., et al. Physics of the Galactic Center Cloud G2, on Its Way toward the Supermassive Black Hole Astrophys. J., 750, 58 (2012)

[45] Schartmann, M., et al. Simulations of the Origin and Fate of the Galactic Center Cloud G2 Astrophys. J., 755, 155 (2012)

[46] Bower G. C., et al. Radio and Millimeter Monitoring of Sgr A*: Spectrum, Variability, and Constraints on the G2 Encounter Astrophys. J., 802, 69 (2015)